EPJ manuscript No.
(will be inserted by the editor)

Landau-Fermi liquidness and s-wave superconducting properties of pressurized gray phosphorus

L. Craco,[1,2] S. S. Carara,[1] and S. Leoni[3]

[1]Institute of Physics, Federal University of Mato Grosso, 78060-900, Cuiabá, MT, Brazil
[2]Leibniz Institute for Solid State and Materials Research Dresden, D-01069, Dresden, Germany
[3]School of Chemistry, Cardiff University, Cardiff, CF10 3AT, UK

the date of receipt and acceptance should be inserted later

Abstract. We investigate the physical properties of compressed gray phosphorus through density functional plus dynamical mean-field theory, showing self-doping and s-wave electronic structure reconstruction. At commensurate electron density the $3p$ spectrum is shown to be almost unaffected by electronic correlations, however upon self-doping largely the normal and superconducting states. These findings provide a microscopic understanding of pressure-induced hole carrier superconductivity on the normal state coherence of s-wave superconductors with well defined Bogoliubov quasiparticles at low temperatures. Upon internal thermalization the s-wave superconducting state loses its phase-coherence.

PACS. 31.15.A Ab initio calculations – 71.10.Fd Lattice fermion models (Hubbard model, etc.) – 71.30.+h Metal-insulator transitions and other electronic transitions

1 Introduction

Interest in black phosphorus (BP) as emerging p-band material has been revitalized after the rising of graphene and topological insulators [1]. At normal conditions bulk BP crystalizes in an orthorhombic ($A17$) structure [2], where layers of six-membered rings with chair conformation are stacked along [010]. In addition to the semiconducting $A17$ structural phase, BP has two pressure-induced crystal structure transitions, the first from orthorhombic to rhombohedral ($A7$) phase at $5.0 \leq P \leq 12.4$ GPa, followed by a simple cubic phase above this pressure range [3,4]. This layered p-band materials allow for sensible changes of physical properties on applying external perturbations [5, 6] Particularly interesting are strain-induced band gap modifications [7], which allow to tune semiconductor BP into anisotropic Dirac semimetal [8], and pressure-induced superconducting phase transitions with $T_c \approx 6 - 13$ K [5, 4,9,10], whose origin could be a fingerprint of electron-phonon coupling mechanism [11].

Superconductivity induced upon intercalation of alkali metals in BP shows a universal critical temperature of 3.8 ± 0.1 K, independent of the synthesized chemical composition [12]. This finding has brought up additional interest about the origin of superconductivity in BP allotropes [13]. High-pressure x-ray diffraction measurements show that around 5 GPa the $A17$ phase partially transforms to a $A7$ phase which coexists with the $A17$ phase between 5 and 8.7 GPa [14] and subsequently becomes single phase at higher pressures. Finally, the $A7$ phase converts to a simple cubic phase at 12.4 GPa [4]. These two high-pressure phases display interesting physical properties, including superconductivity on both $A7$ and simple cubic phases with distinct charge carries [4]. In spite of earlier studies of phonon-mediated superconductivity on pure and doped BP [5,15,16], no detailed understanding of the hole-carrier electronic normal state responsible for the superconducting state in $A7$ gray phosphorus (GP) has been provided so far. In this work we propose a microscopic ingredient for superconductivity [17], namely a pressure-dependent self-doping mechanism [18], leading to fractional $3p$-orbital occupation and hole-carriers in the planar $3p$ orbitals of $A7$ GP.

The relevance of electron-hole carriers on superconductivity is an issue of current interest for both conventional (BCS-electron-phonon mechanism) and unconventional superconductors [17]. Particularly relevant in this context is Ref. [4], showing the importance of hole carriers in developing superconductivity and enhancing the superconducting transition temperature T_c in compressed BP. According to Ref. [4], when hole carriers become dominant in the $A7$ or cubic phases, superconductivity seems to emerge in the former while, in the latter, T_c is enhanced. Here we focus on self-doping inducing electronic reconstruction in the normal [19] and the conventional s-wave superconducting [13] state of $A7$ GP.

The possibility of correlated electron physics in purely p [20] or s [21,22] band systems is to some extent awkward and at the same time very intriguing, since the naive expectation dictates that the itinerance (kinetic energy of p, s-carriers) is appreciable compared to the electron-

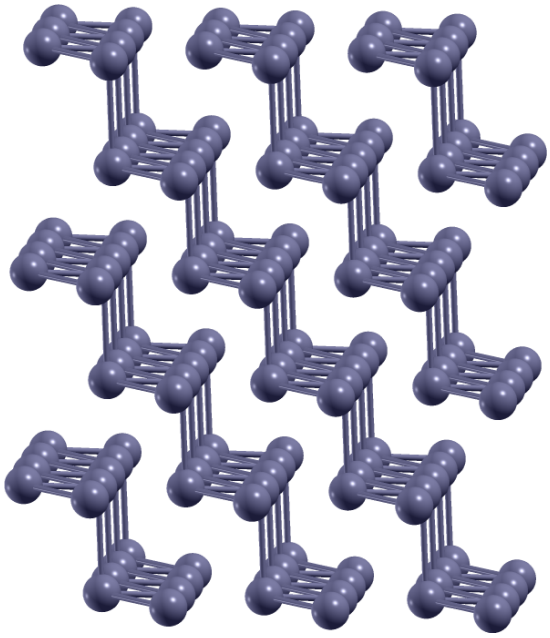

Fig. 1. Layered structure of rhombohedral ($A7$) gray phosphorus at 10.3 GPa.

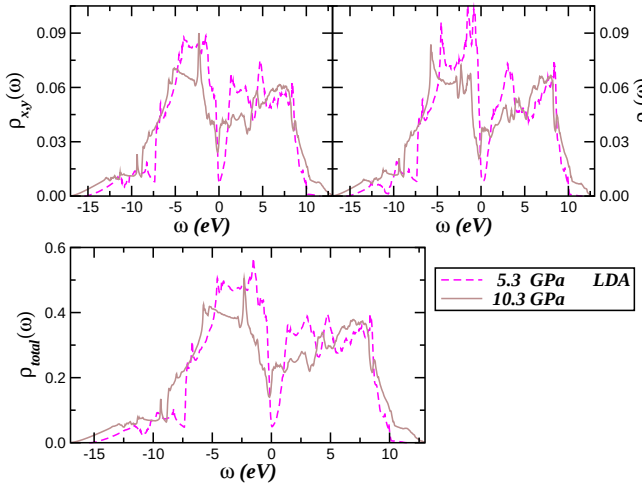

Fig. 2. Comparison between the LDA orbital resolved and total density-of-states (DOS) of $A7$ GP at 5.3 GPa [19] (dashed line) and 10.3 eV (solid line), showing sizable one-particle band broadening under compression. Notice the narrowing of V-valley DOS near the Fermi energy ($E_F = \omega = 0.0$ eV) with increasing pressure.

electron interactions, as distinct from d-band systems, where d electrons reside in much narrower bands (hence the effective U/W is sizable; U and W are, respectively, the on-site Coulomb repulsion and the bare one-particle band width) [23]. Thus, understanding the role played by dynamical on-site Coulomb interactions as the route towards Landau-Fermi liquidness [22,24] in materials with active broad bands is undoubtedly an issue of fundamental interest [25]. With this in place, in an earlier study [19] it was shown that sizable electronic reconstruction qualifies $A7$ GP as an orbital-selective p-band system, hosting renormalized electronic states at low energies. Here, we extend this local-density approximation plus dynamical mean-field theory (LDA+DMFT) work of bulk GP to reveal hidden self-energy effects in superconducting $A7$ GP. Careful investigation of the multi-band (MB) and multi-orbital (MO) electronic dispersions of pure and self-doped GP provides microscopic insights into the electronic behavior of compressed phosphorus allotropes. Additionally, we explore the role played by the s-wave superconducting pairing state [13], showing the emergence of Bogoliubov quasiparticles characteristic of conventional BCS superconductors at low energies [26].

MB and MO physics is inherently complex due to lattice, charge and spin degrees of freedom [23]. These coupled correlations have hampered an integral theoretical approach to real systems. DFT+DMFT [27] allows for a systematic approach to treat static and dynamical many-particle electronic correlation effects both in the normal and superconducting phases [28]. In real systems, external perturbations like pressure, lattice distortions and doping can cause spectacular structural, magnetic and electronic effects. As an illustration thereof, here we study correlation, self-doping, s-wave pairing and thermalization induced electronic reconstructions of compressed $A7$ GP using the DFT+DMFT method, which self-consistently takes into account many-body (strong or not) effects in real solids.

2 Results and discussion

$A17$ BP (space group $Cmca$) is a narrow band gap semiconductor under ambient pressure conditions [29]. Its orthorhombic crystal structure consists of corrugated layers of six-membered rings stacked along [010] direction. $A7$ GP, on the other hand, has a rhombohedral structure (space group $R\bar{3}m$) [30], similar to elemental bismuth [31]. Being an homologue of Bi and As, $A7$ GP is characterized by extended puckered layers of three-connected phosphorus atoms, with shorter distances within each layer than between (111) layers, as shown in Fig. 1.

LDA calculations using crystal structure inputs at 10.3 GPa [4] for superconducting GP were performed using the linear muffin-tin orbitals (LMTO) [32] scheme in the atomic sphere approximation. The corresponding orbital resolved LDA density-of-states (DOS) is shown in Fig. 2. In contrast with GP at 5.3 GPa [19], the orbital resolved and total spectral functions for the $3p$ states show an appreciable one-particle band broadening (≈ 3.7 eV), characterized by large in energy spectral weight transfer (SWT) of both valence and conduction band states with increasing pressure. Also interesting is the reduction of the V-shaped pseudoband gap at low energies, particularly within the in plane x, y orbitals, which is almost symmetric around 0.15 eV binding energy. Thus, upon compression the $3p$ carriers acquire additional itinerance, consistent with enhanced metallicity seen in the normal state electrical transport data [4,10].

In addition to changes in the electron-hole balance [4] near the Fermi energy (E_F), we have identified a small contribution of the $3s$ band to the total electronic structure of $A7$ GP at 10.3 GPa. As shown in Fig. 3 additional residual electronic states are found at and above E_F, implying, as we propose here, a microscopic self-doping mechanism upon compression, where $3p$ electrons are partially transferred to $3s$ electronic states. Since phosphorus is a group 15 element, this self-doping mechanism would necessarily involve partial occupation of the active $3p$ shell. This situation of two active bands with different orbital character and orbital degeneracy provides the underlying microscopic one-band seeds to investigate hidden electron mass enhancement [33] and *s*-wave superconductivity as well as thermalization-induced electronic structure reconstruction of $A7$ GP at high-pressure conditions.

2.1 Role of multi-orbital electronic correlations

Within LDA, the one-electron part of the two-band model Hamiltonian relevant to $A7$ GP is

$$H_0 = \sum_{a,\mathbf{k},\sigma} \varepsilon_a(\mathbf{k}) c^{\dagger}_{a,\mathbf{k},\sigma} c_{a,\mathbf{k},\sigma} + \sum_{i,a,\sigma} (E_a - \mu) n_{i,a,\sigma} \ ,$$

where a denotes the $3s$ and $3p$ bands crossing E_F, μ is the chemical potential and E_a are on-site energies in the real structure under pressure. Here, $\varepsilon_a(\mathbf{k})$ is the two-channel band dispersion, which encodes details of the one-electron LDA band structure. These s and p bands are the relevant one-particle inputs for many-body band structure calculations within LDA+DMFT. In light of non-negligible correlation effects in $A7$ GP [19], here we show how a DMFT treatment of many-particle Coulomb interaction effects properly describe the onset of self-energy corrections in the spectral function of compressed $A7$ GP. This constitute the one-band [34] and MO [27] local interaction terms H^s_{int} and H^p_{int}, respectively. The correlated many-body Hamiltonian $H_{int} = H^s_{int} + H^p_{int} + H^{sp}_{int}$ considered here for $A7$ GP reads

$$H_{int} = U \sum_i n_{s,i,\uparrow} n_{s,i,\downarrow} + U \sum_{i,\alpha} n_{p,i,\alpha,\uparrow} n_{p,i,\alpha,\downarrow} + U' \sum_{p,i,\alpha \neq \beta} n_{p,i,\alpha} n_{p,i,\beta} + U_{sp} \sum_{<ij>} n_{i,s} n_{j,p} \ ,$$

where $\alpha = x, y, z$ denotes the diagonalized $3p$ orbitals, U is the on-site Coulomb interaction, $U' = U - 2J_H$ is the inter-orbital p-band Coulomb interaction, J_H is the corresponding Hund's coupling and U_{sp} is the Madelung term [18].

We evaluate the many-particle Green's functions

$$G_{a,\sigma}(\omega, \mathbf{k}) = \frac{1}{\omega - \Sigma_{a,\sigma}(\omega) - \varepsilon_a(\mathbf{k})}$$

of the many-body Hamiltonian $H = H_0 + H_{int}$ at zero temperature and real frequencies (with $\omega \equiv \omega + i\eta$) using one-band [35] and MO [36] iterated perturbation theory (IPT) impurity solvers for H^s_{int} and H^p_{int}, respectively. Within LDA the one-band dispersions are read off from $\varepsilon_a(\mathbf{k})$. These are inputs for LDA+DMFT which generates Fermi liquid electronic excitations due to self-energy corrections as discussed below. The detailed formulation of IPT for one-band and MO correlated electron systems has already been described in Refs. [35,36] and used in the context of p-band systems [28,37], so we do not repeat the equations here. The IPT *ansatz* is known to account for the correct low- and high-energy behavior of the one-particle spectral functions and self-energies of Hubbard like models in the large-D limit (DMFT). It ensures the Mott-Hubbard metal-insulator transition from a correlated metal to a Mott insulator as a function of the Coulomb interaction U. This interpolative scheme is computationally very efficient, with real frequency output at zero and finite temperatures, enabling the study of electronic structure reconstruction and transport properties of real materials with different magnetically ordered and superconducting phase instabilities. Importantly, our real frequency MO-IPT scheme [36] has a proven record of good semiquantitative agreement with experiments for a range of correlated materials, and it gives results for the spectral functions and self-energies in qualitatively accord with numerical exact continuos-time quantum Monte Carlo (CT-QMC) calculations [38].

Since the role played by electronic correlations in the excitation spectrum of compressed phosphorus allotropes remains not fully understood [39], in Fig. 3 we show LDA+DMFT band- and orbital-resolved spectral functions that emerges from dynamical correlations in bulk GP at 10.3 GPa, for fixed Madelung ($U_{sp} = 0.6U$) and Hund's rule ($J_H = 0.5$ eV) interactions as well as the total electron occupancy $n_{total} = \sum_{a,\sigma} \langle n_{a,\sigma} \rangle = 5.0$. Our choice for U is consistent with a Hartree-Fock estimation of intra-atomic Coulomb energy [40], and has been used in an early study [37] placing bulk BP on the Kondo insulating side of the correlated semiconducting family. Moreover, in our choice of U_{sp} we follow Ref. [41], which has shown that nonlocal interaction terms can be sizable in delocalized broad p band systems like graphene and graphite, with a magnitude reaching up to 60% of the on-site Coulomb interaction. It is worth noting as well that albeit U is considerably large, the U/W parameter ratio used here is small ($W \approx 30.3$ eV is the one-particle LDA bandwidth at 10.3 GPa), placing (as shown in Fig. 3) compressed GP within the Landau-Fermi liquid regime of good metals [22]. In this effectively weakly correlated regime the electronic spectrum of $A7$ GP is almost unaffected by MB and MO dynamical correlations arising from U and U', attesting the stability of the on-particle spectra against sizable Coulomb correlation effects. However, while the spectral lineshape at high energies remains close to that found using the static mean-field (Hartree) approximation, Fig. 3 displays weak, albeit visible, p-band electronic reconstruction between -6 eV to 6 eV, i.e., at the energy window where the dynamical (ω-dependent) self-energies are finite (see our discussion below). Interesting as well is the absence of s-band SWT,

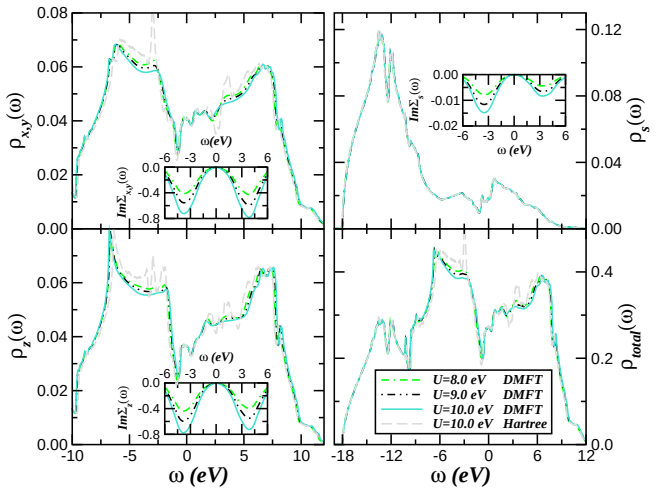

Fig. 3. LDA+DMFT orbital- and band-resolved as well as total DOS of bulk GP at 10.3 GPa for $J_H = 0.5$ eV, $U_{sp} = 0.6U$ and three different values for the on-site Coulomb interaction U, showing the stability of the one-particle spectra against sizable electron correlation effects. The static, LDA+Hartree spectral functions of $A7$ GP are shown for comparison. Inset shows the self-energies imaginary parts, arising from dynamical electron-electron interactions, characteristic of good Landau-Fermi liquid metals.

a signature of vanishing many-body correlation effects in this almost fully polarized electron reservoir.

In order to get realistic insights into the hidden correlated electronic structure evolution due to Landau-Fermi liquidness, in the insets of Fig. 3 we show the frequency dependence of $3p$ and $3s$ self-energy imaginary parts. As seen, all $Im\Sigma_a(\omega)$ follows the ω^2 behavior, intrinsic to Landau-Fermi liquids [42], at low energies. Interestingly, due to strong orbital polarization and lack of inter-orbital Coulomb correlation effects, $Im\Sigma_{3s}(\omega)$ is almost one order of magnitude smaller as compared to $\Sigma_{3p}(\omega)$ self-energies, implying a free electron gas scenario for the $3s$ states of $A7$ GP at 10.3 GPa. Low-energy coherence is also reflected in the linear dependence of $Re\Sigma_a(\omega)$ (not shown), which is relevant to band mass renormalization seen in experiment [33].

In DMFT the quasiparticle residue Z_a, which defines the renormalized Fermi energy of an orbital a, directly yields the effective mass of quasiparticles [42],

$$\frac{m_a^*}{m_e} = \frac{1}{Z_a} = \left(1 - \frac{\partial Re\Sigma_a(\omega)}{\partial\omega}\right)_{\omega=0},$$

where m_e is the free-electron mass. Thus, from the slope of the self-energy real parts at 10.3 GPa we obtain an orbital- and band-dependent effective mass ratio $(m_x^*, m_y^*, m_z^*, m_s^*)/m_e$ of $(1.205, 1.205, 1.199, 1.003)$ for $U = 10.0$ eV, in good agreement with extant data for metallic BP where $m^* = 1.38m_e$ [33]. Interestingly, the effective band mass renormalization we find is also in qualitative good accord with experimental determined values $1.23 < \frac{m^*}{m_e} < 1.28$ for Sodium metal [43], implying similar low-energy Landau-Fermi-liquidness in these two broad electron band systems [22]. Thus, taken together with earlier studies [33, 43], our results in Fig. 3 certify the importance of frequency dependent self-energy corrections for understanding intrinsic electron mass enhancement of real materials.

2.2 Role of pressure-induced self-doping

Under external perturbations like pressure or lattice strain, the hopping matrix elements, the on-site energies and the crystal-field splittings are all renormalized in non-trivial ways. In practice it is difficult to separate these one-body effects, particularly if lattice instabilities are not known a priori. Here, motivated by the dominance of hole carries in superconducting $A7$ GP [4], we adopt the following strategy to derive the electronic state, which might host superconductivity at pressures close to 10.3 GPa. Following an earlier study of electron-phonon mediated superconductivity in hole doped BP [15], where the hole carriers were found to naturally populate the planar bands, resulting in enhanced electron-phonon interaction, we restrict ourselves to the double degenerated x, y orbital sector and consider an orbital-dependent on-site energy term, $H_\delta = \delta \sum_{i,\alpha,\sigma} n_{i,\alpha,\sigma}$ for the $3p_{x,y}$ orbitals in the many-body Hamiltonian of $A7$ GP, i.e., $\bar{H} = H_0 + H_{int} + H_\delta$. In our self-consistent many-particle treatment, we vary $\delta > 0$ in trial steps to simulate the electronic (and hence, self-doping) changes upon compression. Keeping fixed total occupancy, $n_{total} = 5.0$, this choice in H_δ directly leads to $\langle n_{x,y}\rangle > \langle n_z\rangle$ by itself, implying a self-consistent rearrangement of all on-site energies E_a. In our theory, δ_a acts like an orbital field, sensitively controlling the occupancies of each orbital in much the same way as the magnetization of a paramagnet as a function of an external Zeeman field.

Thermodynamically, within our scheme compressed $A7$ GP can be thought as consisting of two $3p$ metallic fluids, one which participates in the superconducting state and another one, which does not. As such, our two-fluid scenario should be applicable to superconductors, where a large portion of spectral weight participates in the superconducting condensate below T_c. Viewed in light of this proposal, our findings below opens up interesting avenues for future studies on two-fluid theories of superconductivity [44].

Fig. 4 shows that small variations of δ with fixed U, J_H and U_{sp} drive appreciable SWT, producing selective electronic reconstruction of the one-particle spectral functions. While the one-particle DOS of the $3s$ band remains similar to the unperturbed $A7$ GP, the $p_{x,y}$ and p_z DOS are clearly affected by the orbital field δ, showing large energy SWT with increasing δ. As expected, while the p_z and $3s$ electronic states are continuously transferred to high binding energies, the $p_{x,y}$ orbital occupancy progressively increases, implying enhanced polarization within the $3p$ orbital states. Thereupon, the V-valleys relevant to valleytronics [45] follows the same trend, with the $p_{x,y}$ crossing E_F for δ between 1.2 and 2.0 eV. For $\delta = 2.0$ eV we find the $p_{x,y}$ orbitals to be 0.102 hole doped, in good ac-

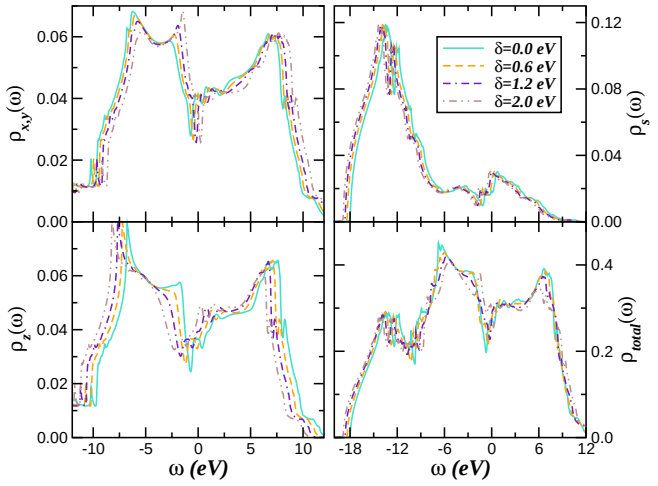

Fig. 4. LDA+DMFT orbital- and band-resolved as well as total DOS of bulk GP at 10.3 GPa for $J_H = 0.5$ eV, $U_{sp} = 6.0$ eV and different values for the orbital-field δ, showing self-doping-induced spectral weight redistribution over large energy scales. Notice the low-energy V-valleys, with the x, y-valley crossing E_F for δ between 1.2 and 2.0 eV.

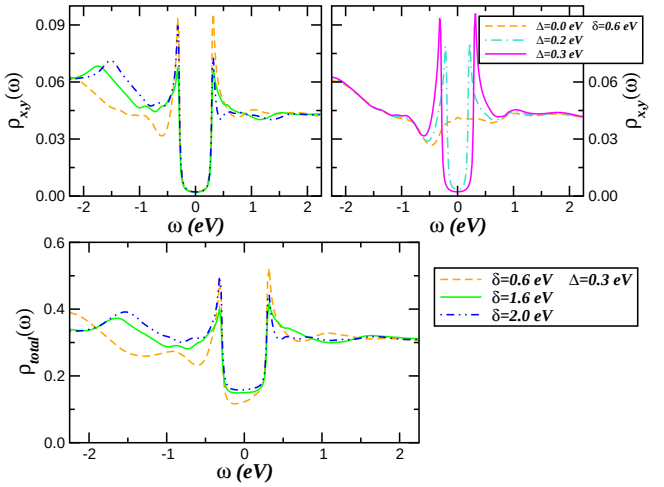

Fig. 5. Left panels display the orbital-resolved and total LDA+DMFT ($U = 10.0$ eV, $J_H = 0.5$ eV, $U_{sp} = 6.0$ eV) spectral functions in the two-fluid [44] s-wave superconducting state of bulk $A7$ GP at 10.3 GPa, showing their changes with increasing the orbital-field δ and fixed pair-field Δ. Notice the particle-hole asymmetry of the sharp Bogoliubov quasiparticles. Right panel shows the normal ($\Delta = 0.0$) and superconducting ($\Delta \neq 0.0$) DOS of the $3p_{x,y}$ orbitals for fixed δ, showing salient superconducting quasiparticles with increasing Δ.

cord with 0.14 hole doped found in Ref. [15] for metallic BP.

2.3 Role of s-wave pairing and lifetime broadening

We now focus on the electronic state which emerges due to s-wave superconductivity in bulk $A7$ GP. In view of the complexity of the problem [13], we only restrict ourselves to a qualitative microscopic many-particle discussion. Since Landau-Fermi liquid quasiparticles are stable excitations in good metals, instabilities to ordered states via BCS-like pairing of well defined Landau-Fermi liquid quasiparticles are tenable. Following the philosophy used earlier [28] for solid O_2 superconductor at extreme high pressure conditions, we restrict ourselves to the $3p_{x,y}$ orbital sector assuming for simplicity an intraband interaction potential V [13]. In this situation the interaction in the Cooper channel reads

$$H_{pair} = \frac{1}{2} V \sum_{\alpha,k,k'} c^{\dagger}_{\alpha,k,\uparrow} c^{\dagger}_{\alpha,-k,\downarrow} c_{\alpha,-k',\downarrow} c_{\alpha,k',\uparrow} \, ,$$

where $\alpha = x, y$. Decoupling H_{pair} in the particle-particle channel [46] gives $H^{MF}_{pair} = \Delta \sum_{\alpha,k} (c^{\dagger}_{\alpha,k,\uparrow} c^{\dagger}_{\alpha,-k,\downarrow} + H.c.)$, with Δ being the induced s-wave pairing potential [26]. As shown below, the two-fluid [44] assumption made here has profound effects in the low energy excitation spectrum within the conventional BCS s-wave superconducting phase.

Aiming to shine light on the changes in the excitation spectrum of bulk $A7$ GP across the superconducting phase transition, we have extended our normal state electronic structure calculation to treat H_{pair} above within the LDA+DMFT formalism for the superconducting state [28]. Using our assumption for the s-wave superconducting pair-field Δ the LDA+DMFT equations are readily extendable to the superconducting regime. As in Ref. [47], the one-particle Green's function have normal and anomalous components yielding renormalized $G_{a,\sigma}$ propagators, which are solved by extending the normal state LDA+DMFT solution to include an explicit pair potential term. Including the pair-field Δ, the LDA+DMFT propagators are written as [28]

$$G_{a,\sigma}(\omega, \mathbf{k}) = \frac{1}{\omega - \Sigma_{a,\sigma}(\omega) - \varepsilon_a(\mathbf{k}) - \frac{\Delta^2}{\omega + \Sigma^{*}_{a,\bar{\sigma}}(\omega) + \varepsilon_a(\mathbf{k})}} \, ,$$

where the $*$ denotes complex conjugation [48]. However, since these equations couple only the planar $3p$-orbitals of $A7$ GP, the opening up of a superconducting gap in a particular x, y-band will not induce secondary gaps in the remaining $3p_z$ and $3s$ bands.

We now describe our results within the s-wave superconducting state of bulk $A7$ GP. Using the normal state LDA+DMFT solution for $\delta = 0.6$ eV, in the right panel of Fig. 5 we show the changes induced by superconductivity in the planar spectral functions of $A7$ GP across the normal-to-superconducting state. As seen, the $3p_{x,y}$ channel is strongly affected by the pairing mechanism. Clear appearance of a superconducting gap and sharp singularities at low-energies are induced across the superconducting phase instability. It is worth mentioning that sharp singularities at low energies as in Fig. 5, the so-called Bogoliubov quasiparticles, are a signature of conventional s-wave superconductivity [26]. Remarkable is

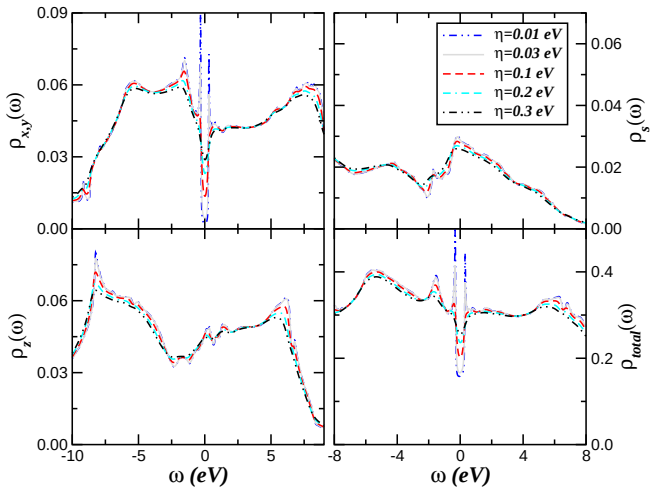

Fig. 6. LDA+DMFT ($U = 10.0$ eV, $J_H = 0.5$ eV, $U_{sp} = 6.0$ eV) spectral functions in the self-doped ($\delta = 2.0$ eV) two-fluid superconducting [44] ($\Delta = 0.3$ eV) phase of $A7$ GP, showing their evolution with increasing the Lorentzian lifetime broadening η. Notice the complete smearing of the Bogoliubov quasiparticles and the gap-closing for $\eta = 0.1$ eV.

the particle-hole asymmetry of the Bogoliubov quasiparticles, with changes in their particle-hole character with increasing the orbital field δ as shown in the left-upper panel of Fig. 5. This is strictly tied to the fact that in $A7$ GP the excitation spectrum is already particle-hole asymmetric. Additionally, while weak SWT from low- to high-energies occurs within the conduction band the valence band states are highly reshaped at energies up to 2 eV binding energy with increasing δ, as clearly seen in the left-upper-panel of Fig. 5. Future tunneling spectroscopy (dI/dV) measurements [49] are called for to corroborate our two-fluid superconducting scenario and the changes in the total one-particle spectral function (Fig. 5 left-lower panel) across the *s*-wave superconducting phase transition in $A7$ GP at pressures close to 10.3 GPa.

However, since Bogoliubov quasiparticles exist only in the coherent superconducting state it is important to inquiry on how stable are the Bogoliubov quasiparticle peaks to thermalization effects [50]. We recall here that internal thermalization usually comes from scatterings due to impurities or residual electron-lattice interactions, which can be included by a finite imaginary part in the retarded Green's function. Therefore, the lifetime broadening $i\eta$ in the single-particle Green's function can be used to simulate thermal smearing induced by internal thermalization of the electron system. With these caveats in mind, in Fig. 6 we show our results for different values for the Lorentzian lifetime broadening [51]. To keep our description realistic here we have chosen η values which are compatible with those reported for broad molecular systems like PF_3, PF_5, and SF_6 with lifetime broadening ranging from 0.3 eV to 0.55 eV [52]. Thus, as seen in Fig. 6 the orbital resolved and total DOS are strongly thermally smeared with increasing η, and as expected the superconducting gap shrinks upon decreasing the lifetime of the Bogoliubov quasiparticles. In this *gap-filling* [48] scenario the Bogoliubov quasiparticles lose their coherence and the corresponding spectral weight fills in the *s*-wave superconducting gap at low energies.

3 Conclusion

In conclusion, we have microscopically studied the electronic structure reconstruction in pressurized $A7$ gray phosphorus using local-density approximation plus dynamical-mean-field theory. Although the main purpose of this paper is to unveil the electronic reconstruction across the superconducting phase instability of normal Landau-Fermi liquids, a major finding of the present study is the effective band mass renormalization, which is in good qualitative agreement with extant data for metallic black phosphorus [33], attesting the importance of treating dynamical correlation effects self-consistently. Implications of our picture for the *s*-wave superconducting state, including the existence of sharp Bogoliubov quasiparticles at low temperatures, are discussed. We demonstrate how the superconducting pairing state involving itinerant ($3p_{x,y}$) orbitals loses its phase-coherence upon thermalization, where the superconducting gap is shown to be continuously filled upon gradual smearing of the Bogoliubov quasiparticles as internal thermalization increases. Our work underlines the importance of local dynamical correlations in this p band system, and holds promise for understanding similar physics in correlated systems where thermalization may occur without temperature [53].

L.C.'s work is supported by CNPq (Grant No. 304035/2017-3). Acknowledgment (L.C. and S.S.C.) is also made to CAPES. S.L. thanks ARCCA Cardiff for computational resources.

Author contribution statement

S.L. carried out the LDA calculations. L.C. designed and carried out the LDA+DMFT study. The authors contributed to the scientific discussions and the preparation of the manuscript, and approved the final version of the manuscript.

Data Availability Statement

This manuscript has no associated data or the data will not be deposited. [Authors comment: The datasets generated and analyzed during the current study are available from the corresponding author upon reasonable request.]

References

1. A. Morita, App. Phys. A **39**, 227 (1986); H. Liu, Y. Du, Y. Deng, and P. D. Ye, Chem. Soc. Rev. **44**, 2732 (2015).

2. F. Xia, H. Wang. J. C. M. Hwang, A. H. Castro Neto, and L. Yang, Nature Review Physics **1**, 306 (2019).
3. T. Kikegawa and H. Iwasaki, Acta Crystallogr., Sect. B: Struct. Sci., Cryst. Eng. Mater. **39**, 158 (1983); I. Shirotani, K. Tsuji, M. Imai, H. Kawamura, O. Shimomura, T. Kikegawa, and T. Nakajima, Phys. Lett. A **144**, 102 (1990); Y. Akahama, M. Kobayashi, and H. Kawamura, Phys. Rev. B **59**, 8520 (1999); S. M. Clark and J. M. Zaug, Phys. Rev. B **82**, 134111 (2010).
4. J. Guo, H. Wang, F. von Rohr, W. Yi, Y. Zhou, Z. Wang, S. Cai, S. Zhang, X. Li, Y. Li, J. Liu, K. Yang, A. Li, S. Jiang, Q. Wu, T. Xiang, R.J. Cava, and L. Sun, Phys. Rev. B **96**, 224513 (2017).
5. J. A. Flores-Livas, A. Sanna, A. P. Drozdov, L. Boeri, G. Profeta, M. Eremets, and S. Goedecker, Phys. Rev. Materials **1**, 024802 (2017).
6. J. Arcudia, R. Kempt, M. E. Cifuentes-Quintal, T. Heine, and G. Merino, Phys. Rev. Lett. **125**, 196401 (2020).
7. R. Fei, V. Tran, and L. Yang, Phys. Rev. B **91**, 195319 (2015); A. S. Rodin, A. Carvalho, and A. H. Castro Neto, Phys. Rev. Lett. **112**, 176801 (2014); G. Qin, Q.-B. Yan, Z. Qin, S.-Y. Yue, H.-J. Cui, Q.-R. Zheng, and G. Su, Sci. Rep. **4**, 6946 (2014).
8. J. Kim, S.S . Baik, S. H. Ryu, Y. Sohn, S. Park, B.-G. Park, J. Denlinger, Y. Yi, H. J. Choi, and K. S. Kim, Science **349**, 723 (2015).
9. I. Shirotani, J. Mikami, T. Adachi, Y. Katayama, K. Tsuji, H. Kawamura, O. Shimomura, and T. Nakajima, Phys. Rev. B **50**, 16274 (1994).
10. X. Li, J. Sun, P. Shahi, M. Gao, A. H. MacDonald, Y. Uwatoko, T. Xiang, J.B. Goodenough, J. Cheng, and J. Zhou, PNAS **115**, 9935 (2018).
11. H. Kawamura, I. Shirotani, and K. Tachikawa, Solid State Commun. **54**, 775 (1985); M. Karuzawa, M. Ishizuka, and S. Endo, J. Phys.: Condens. Matter **14**, 10759 (2002); I. Shirotani, J. Mikami, T. Adachi, Y. Katayama, K. Tsuji, H. Kawamura, O. Shimomura, and T. Nakajima, Phys. Rev. B **50** 16274 (1994).
12. R. Zhang, J. Waters, A. K. Geim, and I. V. Grigorieva, Nature Commun. **8**, 15036 (2017); H. Yuan, L. Deng, B. Lv, Z. Wu, Z. Yang, S. Li, S. Huyan, Y. Ni, J. Sun, F. Tian, D. Wang, H. Wang, S. Chen, Z. Ren, and C. Chu, Mater. Today Phys. **4**, 7 (2018).
13. M. Alidoust, M. Willatzen, and A.-P. Jauho, Phys. Rev. B **99**, 125417 (2019).
14. S. E. Boulfelfel, G. Seifert, Y. Grin, and S. Leoni, Phys. Rev. B **85**, 014110 (2012).
15. Y. Feng, H. Sun, J. Sun, Z. Lu, and Y. You, J. Phys.: Condens. Matter **30**, 015601 (2018).
16. D.F. Shao, W. J. Lu, H. Y. Lv, and Y.P. Sun, Europhys. Letters **108**, 67004 (2014); J.-J. Zhang and S. Dong, 2D Materials **3**, 035005 (2016).
17. See, J. E. Hirsch, J. Supercond. Nov. Magn. **33**, 61 (2020) and references therein.
18. L. Craco, M. S. Laad, S. Leoni, and H. Rosner, Phys. Rev. B **79**, 075125 (2009).
19. L. Craco, T. A. da Silva Pereira, S. R. Ferreira, S. S. Carara, and S. Leoni, Phys. Rev. B 98 (2018) 035114.
20. See, for example, A. J. R. da Silva and L. M. Falicov, Phys. Rev. B **52**, 2325 (1995); J. A. Chan, S. Lany, and A. Zunger, Phys. Rev. Lett. **103**, 016404 (2009); J. Winterlik, G. H. Fecher, C. A. Jenkins, C. Felser, C. Mühle, K. Doll, M. Jansen, L. M. Sandratskii, and J. Kübler, Phys. Rev. Lett. **102**, 016401 (2009); T. Kiss, A. Chainani, H. M. Yamamoto, T. Miyazaki, T. Akimoto, T. Shimojima, K. Ishizaka, S. Watanabe, C.-T. Chen, A. Fukaya, R. Kato, and S. Shin, Nature Commun. **3**, 1089 (2012); see also, N. Tancogne-Dejean and A. Rubio, Phys. Rev. B **102**, 155117 (2020) and references therein.
21. G. Chiappe, E. Louis, E. SanFabián, and J.A. Verges, Phys. Rev. B **75**, 195104 (2007); see also, S. Mandal, K. Haule, K. M. Rabe, and D. Vanderbilt, 2101.03262 (unpublished).
22. See, L. Craco and S. Leoni, Phys. Rev. B **100**, 115156 (2019) and references therein; see also, S. Mandal, K. Haule, K. M. Rabe, and D. Vanderbilt, arXiv:2101.03262 (unpublished).
23. M. Imada, A. Fujimori, and Y. Tokura, Rev. Mod. Phys. **70**, 1039 (1998).
24. T. Kiss, A. Chainani, H. M. Yamamoto, T. Miyazaki, T. Akimoto, T. Shimojima, K. Ishizaka, S. Watanabe, C.-T. Chen, A. Fukaya, R. Kato, and S. Shin, Nature Commun. **3**, 1089 (2012).
25. V. N. Kotov, B. Uchoa, V. M. Pereira, F. Guinea, and A. H. Castro Neto, Rev. Mod. Phys. **84**, 1067 (2012).
26. N. F. Q. Yuan and L. Fu, Phys. Rev. B **97**, 115139 (2018).
27. G. Kotliar, S. Y. Savrasov, K. Haule, V. S. Oudovenko, O. Parcollet, and C. A. Marianetti, Rev. Mod. Phys. **78**, 865 (2006).
28. L. Craco, M. S. Laad, and S. Leoni, Sci. Rep. **7**, 2632 (2017).
29. Z. J. Xiang, G. J. Ye, C. Shang, B. Lei, N. Z. Wang, K. S. Yang, D. Y. Liu, F. B. Meng, X. G. Luo, L. J. Zou, Z. Sun, Y. Zhang, and X. H. Chen, Phys. Rev. Lett. **115**, 186403 (2015).
30. J. C. Jamieson, Science **139**, 1291 (1963).
31. L. Craco and S. Leoni, Sci. Rep. **5**, 13772 (2015).
32. O. K. Andersen, Phys. Rev. B **12**, 3060 (1975).
33. N. Ehlen, A. Sanna, B. V. Senkovskiy, L. Petaccia, A. V. Fedorov, G. Profeta, and A. Grüneis, Phys. Rev. B **97**, 045143 (2018).
34. J. Hubbard, Proc. Roy. Soc. London A **276**, 238 (1963).
35. M. S. Laad, L. Craco, and E. Müller-Hartmann, Phys. Rev. B **64**, 195114 (2001).
36. L. Craco, Phys. Rev. B **77**, 125122 (2008).
37. L. Craco, T. A. da Silva Pereira, and S. Leoni, Phys. Rev. B **96**, 075118 (2017).
38. L. Craco and S. Leoni, Phys. Rev. B **100**, 121101(R) (2019); L. Craco and S. Leoni, Phys. Rev. B **102**, 045142 (2020).
39. X. Wu, H. O. Jeschke, D. Di Sante, F. O. von Rohr, R. J. Cava, and R. Thomale, Phys. Rev. Materials **2**, 034802 (2018).
40. V. Y. Klevets, N. D. Savchenko, T. N. Shchurova, I. I. Opachko, and K. O. Popovic, Functional Materials **20**, 97 (2013).
41. T. O. Wehling, E. Şaşıoğlu, C. Friedrich, A. I. Lichtenstein, M. I. Katsnelson, and S. Blügel, Phys. Rev. Lett. **106** 236805 (2011).
42. A. Georges, G. Kotliar, W. Krauth, and M. J. Rozenberg, Rev. Mod. Phys. **68**, 13 (1996).
43. J. Jensen and E. W. Plummer, Phys. Rev. Lett. **55**, 1912 (1985); I.-W. Lyo and E. W. Plummer. Phys. Rev. Lett. **60**, 1558 (1988).
44. J. Bardeen, Phys. Rev. Lett. **1**, 399 (1958).

45. J. R. Schaibley, H. Yu, G. Clark, P. Rivera, J. S. Ross, K. L. Seyler, W. Yao, and X. Xu, Nature Review Materials **1**, 201655 (2016).
46. R. Fehrenbacher and M. R. Norman, Phys. Rev. Lett. **74** 3884 (1995).
47. M. S. Laad and L. Craco, Phys. Rev. Lett. **103**, 017002 (2009).
48. M. A. Sulangi and J. Zaanen, Phys. Rev. B **98**, 094518 (2018).
49. T. Hanaguri, Y. Kohsaka, J.C. Davis, C. Lupien, I. Yamada, M. Azuma, M. Takano, K. Ohishi, M. Ono, and H. Takagi, Nature Phys. **3**, 865 (2007).
50. See, for example, X. L. Lei, *Balance Equation Approach to Electron Transport in Semiconductors*, World Scientific Publishing Co. Pte. Ltd, Singapore (2008) and references therein.
51. P. M . Richards, Phys. Rev. B **60**, (1999).
52. R. Püttner, T. Marchenko, R. Guillemin, L. Journel, G. Goldsztejn, D. Céolin, O. Takahashi, K. Ueda, A.F. Lago, M. N. Piancastelli, and M. Simon, Phys. Chem. Chem. Phys. **21** 8827 (2019)..
53. D. J. Luitz, R. Moessner, S. L. Sondhi, and V. Khemani, Phys. Rev. X **10**, 021046 (2020).